A&A 521, A16 (2010)
DOI: 10.1051/0004-6361/200913185

Astronomy & Astrophysics

Molecular tracers of filamentary CO emission regions surrounding the central galaxies of clusters

E. Bayet[1], T. W. Hartquist[2], S. Viti[1], D. A. Williams[1], and T. A. Bell[3]

[1] Department of Physics and Astronomy, University College London, Gower Street, London WC1E 6BT, UK
e-mail: [eb;daw]@star.ucl.ac.uk
[2] School of Physics and Astronomy University of Leeds, Leeds LS2 9JT, UK
e-mail: twh@ast.leeds.ac.uk
[3] Department of Astronomy, California Institute of Technology, Pasadena, CA 91125, USA
e-mail: tab@phobos.caltech.edu

Received 26 August 2009 / Accepted 9 July 2010

ABSTRACT

Context. Optical emission is detected from filaments around the central galaxies of clusters of galaxies. These filaments have lengths of tens of kiloparsecs. The emission is possibly due to heating caused by the dissipation of mechanical energy and by cosmic ray induced ionisation. CO millimeter and submillimeter line emissions as well as H_2 infrared emission originating in such filaments surrounding NGC 1275, the central galaxy of the Perseus cluster, have been detected.
Aims. Our aim is to identify those molecular species, other than CO, that may emit detectable millimeter and submillimeter line features arising in these filaments, and to determine which of those species will produce emissions that might serve as diagnostics of the dissipation and cosmic ray induced ionisation.
Methods. The time-dependent UCL photon-dominated region modelling code was used in the construction of steady-state models of molecular filamentary emission regions at appropriate pressures, for a range of dissipation and cosmic ray induced ionisation rates and incident radiation fields.
Results. HCO^+ and C_2H emissions will potentially provide information about the cosmic ray induced ionisation rates in the filaments. HCN and, in particular, CN are species with millimeter and submillimeter lines that remain abundant in the warmest regions containing molecules.
Conclusions. Detections of the galaxy cluster filaments in HCO^+, C_2H, and CN emissions and further detections of them in HCN emissions would provide significant constraints on the dissipation and cosmic ray induced ionisation rates.

Key words. ISM: abundances – intergalactic medium – galaxies: clusters: individual: Perseus – galaxies: individual: NGC 1275 – astrochemistry

1. Introduction

The central galaxies of many clusters of galaxies are surrounded by filaments observed in optical emission lines to extend up to many tens of kiloparsecs (e.g. Crawford et al. 1999; Conselice et al. 2001). The filaments in NGC 1275, the central galaxy of the Perseus cluster, are typically of the order of 100 pc thick. McNamara et al. (1996) suggested that the filaments originate in interactions between the hot intracluster medium and the relativistic plasma associated with the AGN-driven radio features found in and around the central galaxies. Pope et al. (2008b) modelled the filaments of NGC 1275 as material ablated from clouds and dragged by a more diffuse outflow moving away from NGC 1275 at more than 10^3 km s^{-1}. Pope et al. (2008a) suggested that dissipation occurring during the momentum transfer from the diffuse flow to the filaments might power the filamentary emission, an idea related to that of Crawford & Fabian (1992) that turbulent mixing layers play a role in generating the emission. Ferland et al. (2008, 2009) have constructed detailed models of the optical and infrared line emission of filamentary gas heated by similar dissipation and by cosmic ray induced ionisation. They were motivated in part by the difficulties encountered in attempts to match the observed spectra with the results of models in which photoionisation by stellar radiation is assumed to be the dominant heating mechanism (e.g. Johnstone et al. 2007).

Infrared H_2 emission lines trace the optical emission of the filaments (Jaffe et al. 2005). Salomé et al. (2006, 2008a) obtained CO(1−0), and CO(2−1) single dish data on NGC 1275 and its surrounding filaments and they observed HCN(3−2) at the position of 3C84, the radio source located at the centre of the galaxy NGC 1275. These two sets of observations established that both regions contain cold molecular gas. Lim et al. (2008); Salomé et al. (2008b); Ho et al. (2009) have obtained interferometric observations of the CO(2−1) emission of some of the NGC 1275 filaments.

The required heating rates per particle due to dissipation and/or cosmic ray induced ionisation found by Ferland et al. (2009) are several orders of magnitude higher than those in the nearest Milky Way giant molecular clouds, and the required thermal pressures identified by Ferland et al. (2009) (see also Sanders et al. 2004; Sanders & Fabian 2007) are about an order of magnitude higher than those of the envelopes of dense cores associated with low mass star formation. Though the heating and

ionisation rates in the cold molecular regions of the NGC 1275 filaments may be lower than those in the corresponding optical emission regions, they still may greatly exceed those relevant to the nearby Milky Way dense cores. If these rates are relatively high, the chemical composition in the NGC 1275 filaments should differ from that in a typical nearby dense core and may provide a diagnostic of the conditions in the filaments.

Hence, we have examined the chemistry of molecular regions subject to heating rates per volume and cosmic ray ionisation rates per particle in ranges that extend up to those approaching those that, according to Ferland et al. (2009), obtain in the optical emission line regions of the NGC 1275 filaments. Our purpose is to identify those molecular species that may be detectable and to determine which of those species may act as diagnostics of the dissipation heating and of the cosmic ray intensity in the filaments. We shall consider a range of parameters up to those indicated by the observations; however, it is not our purpose here to model the filaments in NGC 1275.

Section 2 contains details of the physical and chemical models that we adopted to describe the molecular component of the filaments. In Sect. 3 we present our results, and Sect. 4 ends the paper with a discussion and some conclusions.

2. The models

We compute the filament chemistry by assuming that the filament may be represented by a steady-state photon-dominated region (a PDR) with constant thermal pressure. To solve for the chemistry in the filament we employ the UCL_PDR time-dependent code, as implemented by Bell et al. (2005, 2007) and Bayet et al. (2009) run for a sufficiently long time to reach steady state. This code operates in one space dimension and computes self-consistently the chemistry and the temperature as functions of depth and time within a semi-infinite slab, taking account of a wide range of heating and cooling processes. In the present work, the code is used to determine the chemical and thermal properties at all depths up to a maximum of about 20 visual magnitudes. For the present work, we have updated the UCL_PDR code to include additional radiative cooling due to rotational transitions of ^{13}CO, C^{18}O, CS, OH and H_2O. The escape probability formalism of de Jong et al. (1980) is used to determine non-LTE level populations and resulting line intensities at each depth- and time-step, in the same manner as for the existing coolants in the code. Collisional rates with H_2 are taken from the Leiden Atomic and Molecular Database (LAMDA; Schöier et al. 2005). The inclusion of these coolants allows the thermal balance to be more accurately determined in warm dense gas at high extinction. The treatment of H_2 self-shielding has also been updated to use the results of detailed calculations performed by Lee et al. (1996). The chemical network links 131 species in over 1700 gas-phase reactions; only H_2 is formed by surface chemistry; freeze-out of species on to grain surfaces is excluded. The UCL_PDR code has been validated against all other commonly used PDR codes (Röllig et al. 2007). The main elemental abundances relative to hydrogen that have been adopted allow for some depletion onto dust, and are C: 1.4×10^{-4}; O: 3.2×10^{-4}; N: 6.5×10^{-5}; S: 1.4×10^{-6}; Mg: 5.1×10^{-6}; and He: 7.5×10^{-2}. The adopted gas:dust mass ratio is 100.

The code requires the adoption of several important parameters that define the local physical conditions. These are (i) the gas number density, or equivalently (since the temperature is determined by the code) the thermal pressure; (ii) the FUV radiation flux impinging on the slab boundary; and (iii) the cosmic ray induced ionisation rate, here assumed to be independent of space and time. Most importantly, in this computation there is also an additional term: (iv) an assumed additional heating source in the filaments, as indicated by Ferland et al. (2009). We discuss each of these parameters in turn.

(i) In most cases the thermal pressure was taken to be $P = k_B(4 \times 10^6$ cm^{-3} K), where k_B is Boltzmann's constant. This value of P is close to the the average values measured by Sanders et al. (2004) for filaments showing optical line emission in NGC 1275 (see also Sanders & Fabian 2007). The Sanders et al. (2004) measurements show a wide scatter, and the average shows an upward gradient in pressure with decreasing cluster radius. Therefore, in some computations we have set the pressure to be one order of magnitude larger than stated above.

(ii) The incident FUV radiation field was taken to be I times the Habing (1968) radiation field mean intensity in the interstellar medium of the Milky Way galaxy. Values of I of 10 and 100 were adopted, on the assumption that the central galaxy in the cluster is, like NGC 1275, a bright galaxy with a central AGN. Of course, obscuration of stellar and AGN radiation affects the intensity impinging on the filaments, and the nature and strength of the incident radiation field are uncertain.

(iii) The cosmic ray induced ionisation rate, ζ, was assigned values in the range of 5×10^{-17} s^{-1} to 5×10^{-13} s^{-1}; the higher values reflect the suggestion of Ferland et al. (2009) for filaments in NGC 1275. Values around 5×10^{-17} s^{-1} are often assumed for clouds within several hundred parsecs of the Sun and even in some studies of extragalactic regions.

(iv) A special feature and most important modification of the present calculations is the inclusion of an unspecified heat source, in addition to the familiar main heat sources of photo-absorption and cosmic ray induced ionisation. The additional heating mechanism, is here – following Ferland et al. (2009) – assumed to be dissipation. We incorporate it by adding a heat source term, H, to the equation of thermal balance. It is time-independent and uniform everywhere, and specifies the thermal energy added per unit time per unit volume by processes not otherwise included in the code. Ferland et al. (2008, 2009) found that H must be within an order of magnitude of 10^{-19} erg cm^{-3} s^{-1} if dissipation powers the observed optical emission regions. Ferland et al. (2009) chose to make their heat source term proportional to gas number density. However, since the physics of the dissipation process is obscure, this choice is arbitrary, and we have set H to be independent of all parameters. The relation between the terms is H_0(Ferland) = H(Bayet)/(n/1 cm^{-3}), or, equivalently, H_0(Ferland) = H(Bayet)(T/4 $\times$ 10^6 K cm^{-3}) for the assumed pressure. Cosmic ray induced ionisation of a region with a hydrogen number density of 10^3 cm^{-3} will be subject to a comparable heating rate (i.e. $H = 10^{-19}$ erg cm^{-3} s^{-1}) due to cosmic rays if ζ is within an order of magnitude of 10^{-12} s^{-1}.

The higher values of our assumed heating rates per unit volume and cosmic ray induced ionisation rates roughly approach the values found by Ferland et al. (2008, 2009) to be compatible with the optical emission line spectra in NGC 1275. However, we limited the upper range of the assumed rates to avoid heating the gas beyond the maximum temperatures at which molecules are abundant. This limiting is consistent with the values of H and ζ decreasing with depth into a filament.

3. Results

The code determines self-consistently the steady-state thermal and chemical properties of a constant-pressure filament subjected to the three heating processes described in Sect. 2;

of these, H and ζ affect the bulk of the filament. In contrast, the effects of I are confined to narrow surface regions, as a comparison of results given in Figs. 2 and 3 for our models 14 and 5 (which differ only in I) confirms. The thermal and chemical properties are computed as functions of A_v, measured from the outer edge of the filament. We present in Table 1 a summary of the models explored and the corresponding thermal and chemical properties at two values of A_v, 3 and 8 mag. These values are intended to represent conditions near the edge and in the dark interior of a filament. We do not list results at $A_v = 8$ for Models 1−5 as they should not differ from those at $A_v = 3$. We include in the final column of Table 1 a list of molecules that are predicted to be fairly abundant in each model (underlined species) and molecules that may be near the current limit of detection (non-underlined species). Evidently, some models are expected to be chemically very rich, while others should be chemically poor. Table 2 contains values at $A_v = 8$ of the fractional abundances of the species. In this section we focus on the results shown in various figures, but the trends that we infer from those figures are also seen in the results in Table 2.

The chemistry varies little with A_v as A_v increases beyond 8. However, the figures that we show give results to higher values of A_v because the visual extinctions of the clumps of which a filament is composed may range to higher values. The maximum A_v from its edge to its centre is probably that of the maximum mass isothermal sphere that is stable against self-gravity. For clumps with dust and elemental abundances like those of of clouds in the local interstellar medium, this A_v is given roughly by

$$A_{v_{max}} = 15 \text{ mag}[n(H_2)T/(4 \times 10^6 \text{ K cm}^{-3})]^{1/2}. \quad (1)$$

This result is based on the expression for the maximum external pressure that can be applied to a Bonner-Ebert sphere without causing it to collapse, the assumption that the pressure in the sphere is roughly constant, and that a column density of 2×10^{21} cm^{-2} hydrogen nuclei corresponds to one magnitude of visual extinction.

The temperature quoted in Table 1 is the kinetic temperature determined self-consistently with the chemistry, given for depths into the filament corresponding to these two values of A_v. The fractional abundance of CO determined by the code at those same depths is also given, as a crude measure of the effectiveness of the chemistry in the filament. It ranges from a value of 1.3×10^{-5}, corresponding to a rich chemistry in which about 10% of available carbon is in CO, to very small values. We summarise in Table 1 the chemistry determined for each model by simply listing molecules familiar from studies of galactic interstellar media; more species than those listed are present. Molecules listed have a fractional abundances of at least 1×10^{-12} (adopted as an arbitrary limit of detectability), and those underlined have fractional abundances of at least 1×10^{-10}. Detections of C_2 and CO_2 will be unlikely, but these molecules are listed for completeness. More information about the dependence of gas density, temperature and chemistry on A_v for particular models is found in Figs. 1−3, described below.

Variations in the additional heating rate: model 10 explores the effect of varying the additional rate, H, over the range 1×10^{-15} to 1×10^{-19} erg cm^{-3} s^{-1}. The high values of H dominate other heating mechanisms and overwhelm the cooling mechanisms. The resulting temperature is so high that very few molecules can survive. Since H is assumed to be independent of depth, this result is true at all depths.

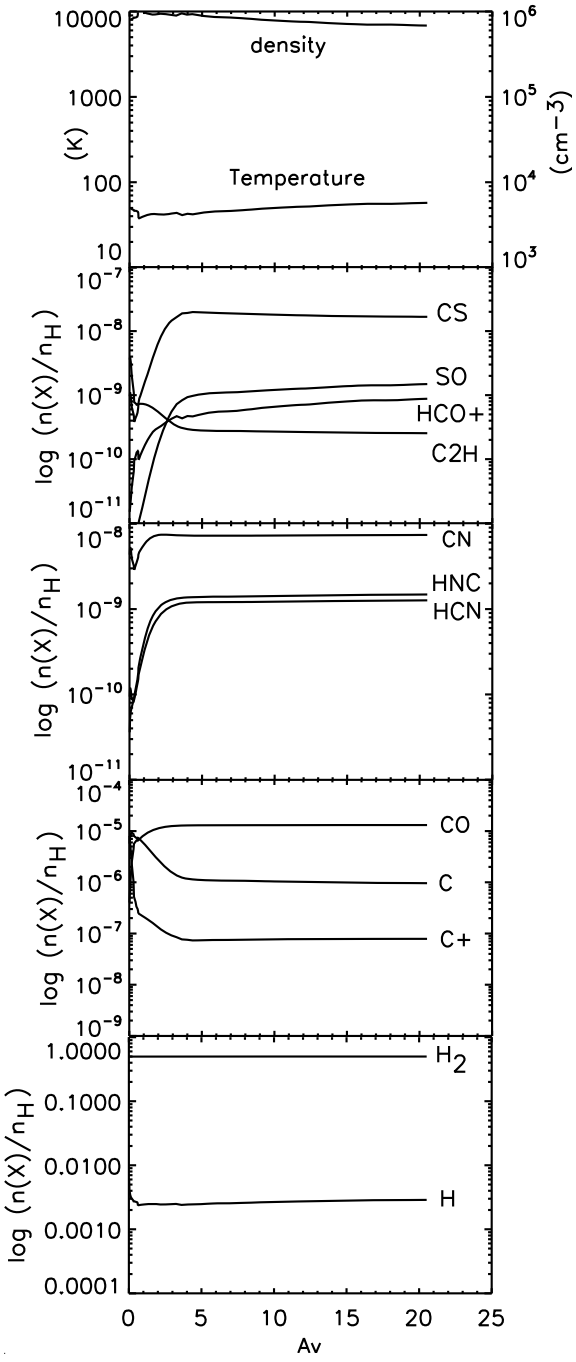

Fig. 1. Fractional abundances with respect to total hydrogen number density of various species (X) as functions of optical depth (A_v), derived from model 16. For each model presented in Figs. 1−3, the plots on *the top* correspond to the density and the temperature profiles. The chemical formula of each molecular species studied is indicated on the plots. When not mentioned, it means that the fractional abundance of X is lower than the arbitrary limit of detectability assumed to be equal to 1×10^{-12}. We have used solid lines for representing the model having an additional heating source of 1×10^{-20} erg cm^{-3} s^{-1} and the dashed lines show the models having an additional heating source of 1×10^{-22} erg cm^{-3} s^{-1}.

For values of H of 1×10^{-20} erg cm^{-3} s^{-1} and smaller, a rich chemistry can exist but is sensitive to the adopted cosmic ray ionisation rate. For example, Models 11 ($H = 1 \times 10^{-20}$ erg cm^{-3} s^{-1}) and 12 ($H = 1 \times 10^{-22}$ erg cm^{-3} s^{-1}) are seen in Table 1 to have almost identical extensive chemistries,

Table 1. Summary of model runs.

Model $A_v = 3$	H (erg cm^{-3} s^{-1})	P (cm^{-3} K)	I (Habing)	ζ (s^{-1})	T (K)	CO/H	Interesting molecules
1	1×10^{-20}	4×10^{6}	100	5×10^{-14}	2866.9	1.7×10^{-9}	O, OH, H_3^+, C^+, CN, C, H_2, H, H_2O, CO
2	1×10^{-22}	4×10^{6}	100	5×10^{-14}	91.4	4.1×10^{-6}	H_3^+, C^+, CN, C, H_2, H, H_2O, HCN, C_2, H_3O^+, C_2H, HCO^+, CO, O, OH, CO_2, HNC
3	1×10^{-20}	4×10^{6}	100	5×10^{-15}	68.2	6.5×10^{-6}	H_3^+, C^+, CN, C, H_2, H, H_2O, HCN, NH_3, C_2, H_3O^+, C_2H, OCN, SO, CS, HCO^+, CO, O, OH, H_2CO, CO_2, HNC, HNO
4	1×10^{-22}	4×10^{6}	100	5×10^{-15}	51.3	3.5×10^{-6}	H_3^+, C^+, CN, C, H_2, H, H_2O, HCN, NH_3, C_2, H_3O^+, C_2H, OCN, SO, CS, HCO^+, CO, O, OH, H_2CO, CO_2, HNC, HNO
5	1×10^{-22}	4×10^{6}	100	5×10^{-17}	25.3	1.2×10^{-5}	H_3^+, C^+, CN, HCO, C, H_2, H, H_2O, HCN, NH_3, C_2, H_3O^+, C_2H, OCN, HCS, H_2CS, NS, SO, CS, HCO^+, CO, O, OH, H_2CO, HS, CO_2, HNC, HNO
6	1×10^{-22}	4×10^{6}	10	5×10^{-13}	2479.6	9.9×10^{-11}	H_3^+, C^+, C, H_2, H, H_2O, CO, O, OH
7	1×10^{-23}	4×10^{6}	10	5×10^{-13}	2456.1	1.0×10^{-10}	H_3^+, C^+, C, H_2, H, H_2O, CO, O, OH
8	1×10^{-20}	4×10^{6}	10	5×10^{-14}	87.5	3.9×10^{-6}	C^+, CN, C, H_2, H, H_2O, HCN, C_2, H_3O^+, C_2H, HCO^+, CO, O, OH, CO_2, HNC
9	1×10^{-22}	4×10^{6}	10	5×10^{-14}	86.2	3.8×10^{-6}	H_3^+, C^+, CN, C, H_2, H, H_2O, HCN, C_2, H_3O^+, C_2H, HCO^+, CO, O, OH, CO_2, HNC
10	1×10^{-15}-1×10^{-19}	4×10^{6}	10	5×10^{-15}	10000.0	5.35×10^{-14}	C^+, C, H_2, H, O, OH
11	1×10^{-20}	4×10^{6}	10	5×10^{-15}	61.8	5.8×10^{-6}	H_3^+, C^+, CN, C, H_2, H, H_2O, HCN, NH_3, C_2, H_3O^+, C_2H, OCN, SO, CS, HCO^+, CO, O, OH, H_2CO, CO_2, HNC, HNO
12	1×10^{-22}	4×10^{6}	10	5×10^{-15}	51.0	3.7×10^{-6}	H_3^+, C^+, CN, C, H_2, H, H_2O, HCN, NH_3, C_2, H_3O^+, C_2H, OCN, SO, CS, HCO^+, CO, O, OH, H_2CO, CO_2, HNC, HNO
13	0	4×10^{6}	10	5×10^{-15}	50.8	3.7×10^{-6}	H_3^+, C^+, CN, C, H_2, H, H_2O, HCN, NH_3, C_2, H_3O^+, C_2H, OCN, SO, CS, HCO^+, CO, O, OH, H_2CO, CO_2, HNC, HNO
14	1×10^{-22}	4×10^{6}	10	5×10^{-17}	13.8	1.4×10^{-5}	H_3^+, C^+, CN, HCO, C, H_2, H, H_2O, HCN, NH_3, C_2, H_2S, H_3O^+, C_2H, OCS, OCN, HCS, H_2CS, NS, SO, CS, HCO^+, CO, O, OH, H_2CO, HS, CO_2, HNC, HNO
15	0	4×10^{6}	10	5×10^{-17}	12.4	1.4×10^{-5}	H_3^+, C^+, CN, HCO, C, H_2, H, H_2O, HCN, NH_3, C_2, H_2S, H_3O^+, C_2H, OCS, OCN, HCS, H_2CS, NS, SO, CS, HCO^+, CO, O, OH, H_2CO, HS, CO_2, HNC, HNO
16	1×10^{-20}	4×10^{7}	10	5×10^{-15}	43.8	1.3×10^{-5}	H_3^+, C^+, CN, C, H_2, H, H_2O, HCN, NH_3, C_2, H_2S, H_3O^+, C_2H, OCS, OCN, HCS, H_2CS, NS, SO, CS, HCO^+, CO, O, OH, H_2CO, HS, CO_2, HNC, HNO, C_2N, H_2CN
17	1×10^{-22}	4×10^{7}	10	5×10^{-15}	41.1	1.3×10^{-5}	H_3^+, C^+, CN, C, H_2, H, H_2O, HCN, NH_3, C_2, H_2S, H_3O^+, C_2H, OCS, OCN, HCS, H_2CS, NS, SO, CS, HCO^+, CO, O, OH, H_2CO, HS, CO_2, HNC, HNO, C_2N, H_2CN
18	1×10^{-20}	4×10^{6}	10	5×10^{-17}	74.8	1.3×10^{-5}	H_3^+, C^+, CN, C, H_2, H, H_2O, HCN, NH_3, C_2, H_3O^+, C_2H, OCS, OCN, HCS, H_2CS, NS, SO, CS, HCO^+, CO, O, OH, H_2CO, HS, CO_2, HNC, HNO, H_2CN
$A_v = 8$							
8	1×10^{-20}	4×10^{6}	10	5×10^{-14}	101.7	4.9×10^{-6}	H_3^+, C^+, CN, C, H_2, H, H_2O, HCN, NH_3, C_2, H_3O^+, C_2H, SO, HCO^+, CO, O, OH, CO_2, HNC
9	1×10^{-22}	4×10^{6}	10	5×10^{-14}	99.1	4.7×10^{-6}	H_3^+, C^+, CN, C, H_2, H, H_2O, HCN, NH_3, C_2, H_3O^+, C_2H, SO, HCO^+, CO, O, OH, CO_2, HNC
10	1×10^{-15}-1×10^{-19}	4×10^{6}	10	5×10^{-15}	10000.0	5.36×10^{-14}	C^+, C, H_2, H, O, OH
11	1×10^{-20}	4×10^{6}	10	5×10^{-15}	78.7	8.3×10^{-6}	H_3^+, C^+, CN, C, H_2, H, H_2O, HCN, NH_3, C_2, H_3O^+, C_2H, OCN, SO, CS, HCO^+, CO, O, OH, H_2CO, CO_2, HNC, HNO
12	1×10^{-22}	4×10^{6}	10	5×10^{-15}	60.2	5.6×10^{-6}	H_3^+, C^+, CN, C, H_2, H, H_2O, HCN, NH_3, C_2, H_3O^+, C_2H, OCN, SO, CS, HCO^+, CO, O, OH, H_2CO, CO_2, HNC, HNO
13	0	4×10^{6}	10	5×10^{-15}	59.9	5.5×10^{-6}	H_3^+, C^+, CN, C, H_2, H, H_2O, HCN, NH_3, C_2, H_3O^+, C_2H, OCN, SO, CS, HCO^+, CO, O, OH, H_2CO, CO_2, HNC, HNO
14	1×10^{-22}	4×10^{6}	10	5×10^{-17}	15.0	1.4×10^{-5}	H_3^+, C^+, CN, HCO, C, H_2, H, H_2O, HCN, NH_3, C_2, H_2S, H_3O^+, C_2H, OCS, OCN, H_2CS, CH_3OH, NS, SO, CS, HCO^+, CO, O, OH, H_2CO, HS, CO_2, HNC, HNO
15	0	4×10^{6}	10	5×10^{-17}	13.4	1.4×10^{-5}	H_3^+, C^+, CN, HCO, C, H_2, H, H_2O, HCN, NH_3, C_2, H_2S, H_3O^+, C_2H, OCS, OCN, H_2CS, CH_3OH, NS, SO, CS, HCO^+, CO, O, OH, H_2CO, HS, CO_2, HNC, HNO
16	1×10^{-20}	4×10^{7}	10	5×10^{-15}	47.5	1.3×10^{-5}	H_3^+, C^+, CN, C, H_2, H, H_2O, HCN, NH_3, C_2, H_2S, H_3O^+, C_2H, OCS, OCN, HCS, H_2CS, NS, SO, CS, HCO^+, CO, O, OH, H_2CO, HS, CO_2, HNC, HNO, C_2N
17	1×10^{-22}	4×10^{7}	10	5×10^{-15}	45.2	1.3×10^{-5}	H_3^+, C^+, CN, C, H_2, H, H_2O, HCN, NH_3, C_2, H_2S, H_3O^+, C_2H, OCS, OCN, HCS, H_2CS, NS, SO, CS, HCO^+, CO, O, OH, H_2CO, HS, CO_2, HNC, HNO, C_2N
18	1×10^{-20}	4×10^{6}	10	5×10^{-17}	63.3	1.4×10^{-5}	H_3^+, C^+, CN, C, H_2, H, H_2O, HCN, NH_3, C_2, H_2S, H_3O^+, C_2H, OCS, OCN,H_2CS, NS, SO, CS, HCO^+, CO, O, OH, H_2CO, HS, CO_2, HNC, HNO

Notes. When the symbol for a molecular species is underlined, its fractional abundance is above 1×10^{-10} otherwise it is simply above 1×10^{-12} (limit of detectability assumed). The temperature mentioned in the Col. 6 is self-consistently determined at the particular value of A_v shown.

Table 2. Fractional abundances with respect to the total number of H-nuclei for models 8−18 at A_v = 8 mag.

Model:	8	9	10	11	12	13	14	15	16	17	18
Species											
H_3^+	2.84(–8)	2.76(–8)	–	5.36(–8)	3.19(–8)	3.16(–8)	9.09(–10)	8.35(–10)	1.34(–8)	1.27(–8)	2.74(–9)
C^+	6.11(–6)	6.18(–6)	1.40(–5)	1.70(–6)	1.96(–6)	1.97(–6)	6.01(–10)	5.32(–10)	7.58(–8)	7.43(–8)	3.27(–9)
CN	9.56(–11)	9.33(–11)	–	2.28(–9)	1.99(–9)	1.99(–9)	1.81(–10)	1.53(–10)	7.24(–9)	7.23(–9)	8.01(–10)
HCO	–	–	–	–	–	–	2.61(–12)	2.56(–12)	–	–	–
C	3.23(–6)	3.36(–6)	2.06(–7)	4.19(–6)	6.66(–6)	6.73(–6)	4.48(–9)	4.05(–9)	1.07(–6)	1.08(–6)	3.15(–8)
H_2O	2.30(–7)	2.18(–7)	–	9.90(–8)	5.29(–8)	5.22(–8)	4.97(–7)	5.14(–7)	1.81(–7)	1.78(–7)	3.82(–7)
HCN	2.87(–12)	2.68(–12)	–	9.25(–11)	4.58(–11)	4.51(–11)	1.60(–9)	2.02(–9)	1.21(–9)	1.20(–9)	4.61(–10)
NH_3	1.22(–12)	1.13(–12)	–	1.15(–10)	4.50(–11)	4.42(–11)	5.46(–8)	6.85(–8)	3.12(–9)	3.02(–9)	1.66(–8)
H_2S	–	–	–	–	–	–	3.70(–11)	4.07(–11)	1.54(–12)	1.60(–12)	1.01(–11)
H_3O^+	3.14(–9)	2.94(–9)	–	8.10(–10)	4.23(–10)	4.16(–10)	2.41(–11)	2.33(–11)	1.89(–10)	1.77(–10)	5.11(–11)
C_2H	1.98(–12)	2.00(–12)	–	2.84(–10)	2.95(–10)	2.95(–10)	5.21(–12)	5.11(–12)	2.74(–10)	2.76(–10)	3.43(–12)
OCS	–	–	–	–	–	–	1.21(–10)	1.50(–10)	2.05(–11)	2.19(–11)	1.125(–11)
OCN	–	–	–	8.66(–12)	3.80(–12)	3.74(–12)	2.54(–8)	3.26(–8)	4.82(–10)	5.07(–10)	3.52(–10)
HCS	–	–	–	–	–	–	–	–	3.55(–11)	3.74(–11)	–
H_2CS	–	–	–	–	–	–	6.82(–11)	6.72(–11)	2.01(–10)	2.13(–10)	4.92(–11)
CH_3OH	–	–	–	–	–	–	1.99(–12)	2.44(–12)	–	–	–
NS	–	–	–	–	–	–	3.54(–12)	2.96(–12)	5.64(–12)	5.42(–12)	1.13(–11)
SO	1.21(–12)	1.08(–12)	–	2.03(–11)	4.84(–12)	4.70(–12)	3.60(–8)	3.56(–8)	1.14(–9)	1.085(–9)	2.03(–8)
CS	–	–	–	3.65(–10)	3.59(–10)	3.58(–10)	4.76(–8)	4.67(–8)	1.86(–8)	1.93(–8)	4.64(–8)
HCO^+	4.05(–10)	3.72(–10)	–	8.80(–10)	2.94(–10)	2.87(–10)	5.32(–11)	4.75(–11)	5.94(–10)	5.39(–10)	2.62(–10)
CO	4.86(–6)	4.66(–6)	–	8.31(–6)	5.57(–6)	5.50(–6)	1.39(–5)	1.38(–5)	1.30(–5)	1.30(–5)	1.41(–5)
O	2.53(–5)	2.56(–5)	3.18(–5)	2.29(–5)	2.60(–5)	2.60(–5)	9.13(–6)	9.25(–6)	1.73(–5)	1.73(–5)	1.18(–5)
OH	1.48(–6)	1.40(–6)	1.67(–12)	4.08(–7)	2.23(–7)	2.20(–7)	2.58(–8)	2.59(–8)	1.17(–7)	1.10(–7)	3.77(–8)
H_2CO	–	–	–	2.93(–11)	2.23(–11)	2.21(–11)	5.13(–11)	5.06(–11)	5.18(–10)	5.25(–10)	3.92(–11)
HS	–	–	–	–	–	–	1.23(–11)	1.21(–11)	8.89(–12)	8.78(–12)	1.82(–11)
HNC	1.22(–11)	1.15(–11)	–	2.27(–10)	1.31(–10)	1.29(–10)	9.33(–10)	1.15(–9)	1.41(–9)	1.40(–9)	4.22(–10)
HNO	–	–	–	6.61(–11)	4.93(–11)	4.88(–11)	4.22(–10)	2.84(–10)	1.99(–9)	1.95(–9)	7.43(–10)
C_2N	–	–	–	–	–	–	–	–	1.77(–12)	1.75(–12)	–

Notes. The power is indicated in parenthesis such as $a(b) = a \times 10^b$. When a dash is used, it means that the fractional abundance is below our assumed limit of detectability of 1×10^{-12}.

while Model 13 ($H = 0$) is indistinguishable from Model 12. Thus, $H = 1 \times 10^{-20}$ erg cm^{-3} s^{-1} appears to be a critical value; above this value, the heating is so great that the chemistry is largely suppressed, while below this value a rich chemistry occurs and is insensitive to H. However, as mentioned above, the value of ζ affects the richness of the chemistry for a particular value of H. For example, Models 11 and 8 (both with $H = 1 \times 10^{-20}$ erg cm^{-3} s^{-1}) differ in ζ (5×10^{-15} s^{-1} and 5×10^{-14} s^{-1}, respectively); Model 11 is distinctly richer in chemistry.

For heating due to dissipation to exceed that due to cosmic ray induced ionisation H must exceed a value given roughly by

$$H_{\rm min} = 1 \times 10^{-22} \text{ erg cm}^{-3} \text{ s}^{-1} \times (n(\text{H}_2)T)/(4 \times 10^6 \text{ K cm}^{-3}) \times (T/100 \text{ K})^{-1} \times \zeta/(5 \times 10^{-17} \text{ s}^{-1}). \quad (2)$$

This result is based on the assumption that one ionisation produces about 40 eV of thermal energy.

Figure 1 shows the dependences of the total number density and temperature in the gas, and the chemical abundances, as functions of depth for Model 16. This model may have plausible values of the physical parameters. It shows a modest temperature and a rich chemistry. Evidently, the familar galactic tracers CS, SO, HCO^+, C_2H, CN, HNC and HCN should be useful for determining the nature of the intracluster material in cases where the parameters are similar to those of Model 16.

Figure 2 compares the chemistries predicted by two Models, 14 and 18, which both have low values of ζ but differ strongly in H (1×10^{-22} erg cm^{-3} s^{-1} and 1×10^{-20} erg cm^{-3} s^{-1}, respectively). Some spikes are seen for Model 18 because the heating is only just matched by the cooling, and the balance is thus computationally delicate. Both models show a rich chemistry, but there are some physical and chemical differences. For example, the important tracer ion HCO^+ is more abundant in Model 18; and the molecules CN, HCN and HNC have a different priority order of abundance in the two models, caused by the higher temperature in Model 18.

Variations in the cosmic ray ionisation rate: the value of ζ is an important parameter both for the chemistry and for the thermal balance. The cases with highest ζ examined here are Models 6 and 7, with $\zeta = 5 \times 10^{-13}$ s^{-1}. The value of H is low in both Models (1×10^{-22} erg cm^{-3} s^{-1} and 1×10^{-23} erg cm^{-3} s^{-1}, respectively), so the major heat input is from the cosmic rays. The temperature is high and the chemistry is largely suppressed; even CO is held down to a fractional abundance of about 1×10^{-10}. The high ζ but low CO abundance leads to a significant H_3^+ abundance. This suppression of the chemistry for high ζ is in agreement with the findings of Lepp & Dalgarno (1996)(see also Lepp & Tiné 1998).

Figure 3 compares results from Models 5 and 12 which both have low values of H (1×10^{-22} erg cm^{-3} s^{-1}), but strongly differing values of ζ (5×10^{-17} s^{-1} and 5×10^{-15} s^{-1}, respectively). Both are chemically rich (Model 5 is slightly richer) but there are significant differences. For example, Model 5 has very much higher SO and CS abundances than Model 12, while the reversed is true for C_2H and HCO^+. The abundance order of priority of CN, HNC and HCN is reverse between Models 5 and 12, with the abundance of CN being one order of magnitude larger in the high ζ case, Model 12. This case also has abundant atomic

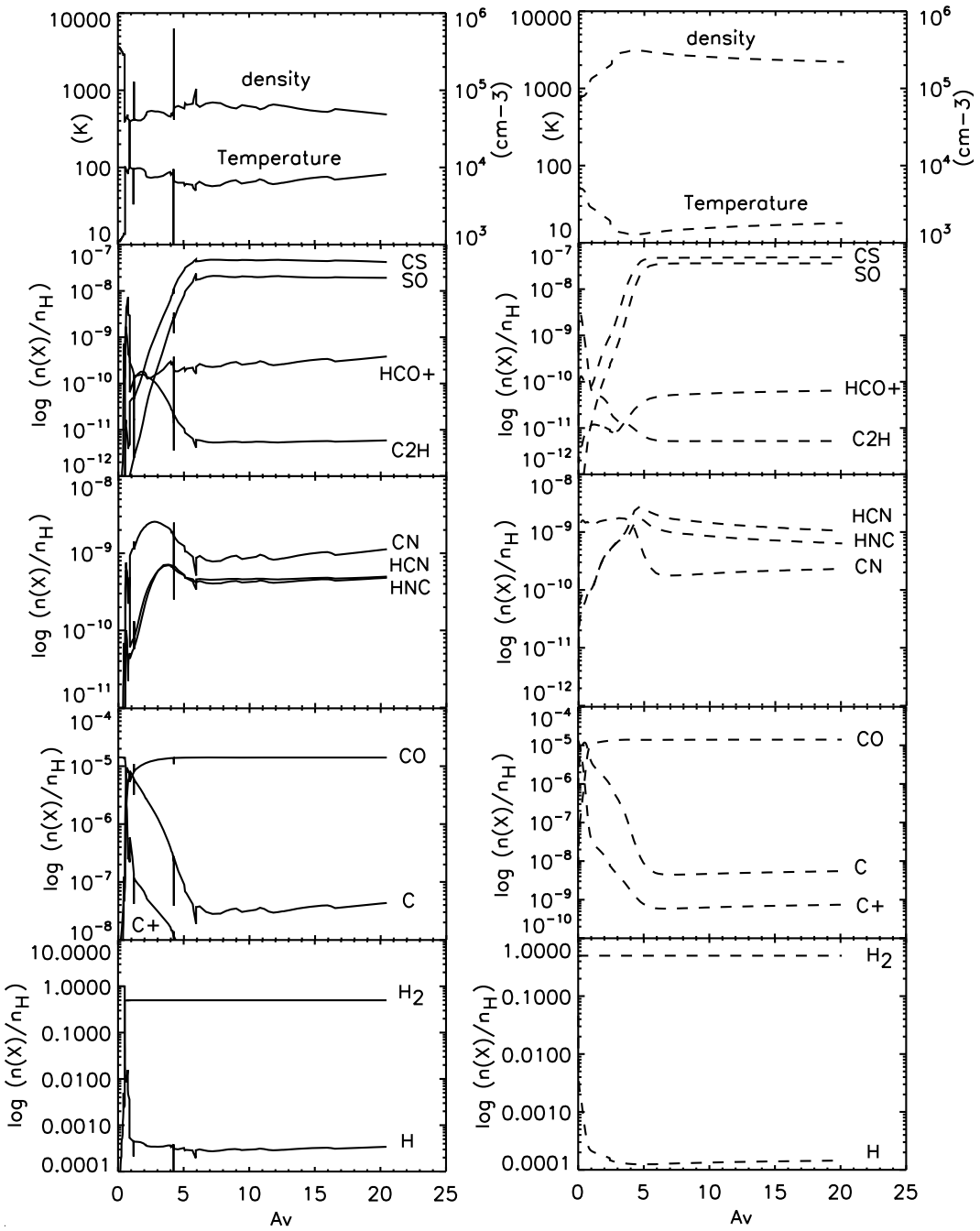

Fig. 2. Fractional abundances with respect to total hydrogen number density of various species (X) as functions of optical depth (A_v), derived from Model 18 (*left*) and Model 14 (*right*). We have used solid lines for representing the models having an additional heating source of 1×10^{-20} erg cm^{-3} s^{-1} (i.e. Model 18) and, as previously, the dashed lines show the models having an additional heating source of 1×10^{-22} erg cm^{-3} s^{-1} (i.e. Model 14). See caption of Fig. 1.

species H, C and C$^+$ relative to Model 5. It is well known that the H:H$_2$ ratio, maintained in this case by the high ζ, has a significant effect on the chemistry (Rawlings et al. 2002).

Other variations: the adopted pressure, P, has a limited effect on the thermal and chemical behaviour. Comparing Models 11 and 16, or 12 and 17 (which differ only in P) shows that the temperature is slightly lower at higher pressure (as expected since the cooling is more effective), and that this slight difference generates a difference in the chemistry, with the cooler models being very slightly chemically richer.

The ambient radiation field can be an important source of heat at the cloud edge, comparable to $H = 1 \times 10^{-20}$ erg cm^{-3} s^{-1} in unshielded situations. However, this heating effect decays rapidly with depth into the cloud. For the higher values of I explored here, $I = 100$, the radiation field may still be making a contribution to the heating, even at $A_v = 3$. We show in Table 3 a comparison of the heating rates from the main heating sources in several models at both low and high A_v. Evidently, the cosmic rays and the dissipation (i.e. H) are the most important sources. Comparing Models 4 and 12 shows that the larger value of I in Model 4 can be making no difference when

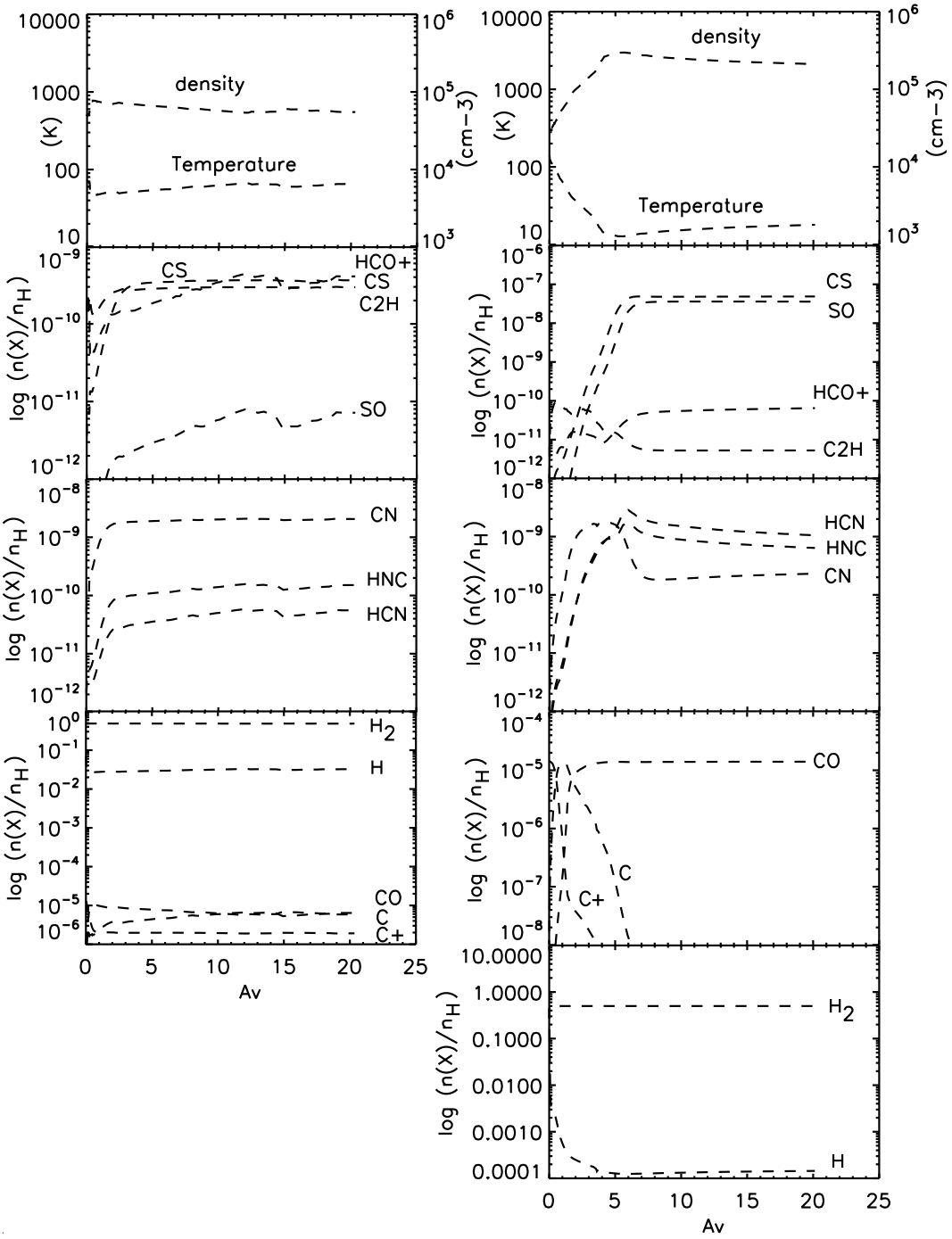

Fig. 3. Fractional abundances with respect to total hydrogen number density of various species (X) as functions of optical depth (A_v), derived from Model 12 (*left*) and Model 5 (*right*). As previously, the dashed lines show the models having an additional heating source of 1×10^{-22} erg cm^{-3} s^{-1} (i.e. both Models 12 and 5). Here the difference between the models is the cosmic ray ionisation rate used ($\zeta = 5 \times 10^{-15}$ s^{-1} for Model 12 whereas Model 5 has $\zeta = 5 \times 10^{-17}$ s^{-1}) and the FUV radiation field ($I = 10$ Habing for Model 12 whereas Model 5 shows $I = 100$ Habing). See caption of Fig. 1 and text in Sect. 3.

$\zeta = 5 \times 10^{-15}$ s^{-1}, because cosmic rays dominate the heating in these cases. However, comparing Models 5 and 14, both of which have a low value of ζ, 5×10^{-17} s^{-1}, we see that the higher value of I in Model 5 increases the temperature relative to Model 12 – though not enough to make a difference to the chemistry.

At low A_v, Model 1 shows a surprisingly high temperature and poor chemistry compared to a similar model, 8, with lower value of I. Evidently, the radiation field can have a significant effect in the boundary layers of filaments. This comparison emphasises the "flip-flop" effect; a rich chemistry provides many coolants that generate a low temperature, enhancing the chemistry; and vice-versa. Model 1 is expected to show a much lower temperature at greater depths.

4. Conclusions

The self-consistent treatment of thermal and chemical behaviour tends to lead to one of two alternative regimes: low temperature and rich chemistry, or high temperature and poor

Table 3. Main contributors to the heating rates (erg s^{-1} cm^{-3}) in several models (See Table 1).

A_v = 3 mag			
heating sources	Model 1	Model 8	Model 18
FUV	8.8×10^{-24}	8.8×10^{-23}	1.7×10^{-23}
H	1.0×10^{-20}	1.0×10^{-20}	1.0×10^{-20}
Cosmic rays	1.0×10^{-21}	3.4×10^{-20}	4.0×10^{-23}
A_v = 8 mag			
heating sources	Model 14	Model 8	Model 18
FUV	8.8×10^{-26}	7.6×10^{-27}	1.3×10^{-27}
H	1.0×10^{-22}	1.0×10^{-20}	1.0×10^{-20}
Cosmic rays	2.0×10^{-22}	2.9×10^{-20}	4.7×10^{-23}

chemistry. The rich chemistry provides efficient cooling, enhancing the chemistry, while elevated temperatures suppress the chemistry and destroy coolants.

The parameter regime that is covered in this study shows that there are two main contributors to the heating, the additional source *H* and cosmic rays. The ambient radiation field is unlikely to be dominant and is in any case confined to a skin-effect of a few visual magnitudes into the filament. The density of the filament has been assumed in our calculations to be uniform. Of course, is the gas is clumpy, then the radiation fields may play a larger role at greater depths than in the homogeneous case. Varying the pressure from the adopted value has only a minor effect on the chemistry.

Very high values of H, $\geq 1 \times 10^{-20}$ erg cm^{-3} s^{-1}, tend to suppress the chemistry and consequent coolants, so temperatures approach those of HII regions. Very high cosmic ray ionisation rates, $\geq 1 \times 10^{-13}$ s^{-1}, have a similar effect. For $H \lesssim 1 \times 10^{-20}$ erg cm^{-3} s^{-1} and $\zeta \lesssim 1 \times 10^{-14}$ s^{-1}, the heating and consequent chemical effects of the two processes combine.

These rates considerably exceed the typical rates in dark clouds near to the Sun (and may be even higher in the filamentary optical regions). If these are representative of the conditions in filamentary molecular regions, then there are many molecular species that should be abundant and useful as tracers of the physical conditions. CS, CN and HNC decline less in abundance with increasing heating and ionisation rates than many species. C_2H and HCO^+ increase in abundance with cosmic ray ionisation rate for a wide range of rates but become less abundant for very high rates. The ratio of those two abundances decreases with increasing dissipative heating rate. N_2H^+, a molecule used successfully to trace dense molecular clouds in the Galaxy, is notable by its absence from our predictions.

In our recommendations for molecular line searches in cluster filaments, we have been guided by the molecular abundances predicted by our computations and by their sensitivity to changes in heating and ionisation rates. The construction of detailed models will be possible once more observational data exist. However, we can give some indication of the expected range of HCO^+, C_2H and CN line intensities, assuming no beam dilution. To do so, we have used RADEX[1] developed by van der Tak et al. (2007), for plane-parallel geometry, for Models 12, 14, 16 and 18 seen in Figs. 2 and 3. We have obtained for the $HCO^+(1-0)$ transition, values ranging from 0.62 K km s^{-1} (Model 14) to 5.6 K km s^{-1} (Model 16). For the $HCO^+(5-4)$ line, values range from 0.2 K km s^{-1} (Models 12 and 18) to 4.2 K km s^{-1} (Model 16). For the CN(1−0) line, we have obtained values from 0.2 K km s^{-1} (Model 14) to 7.6 K km s^{-1} (Model 16). For the CN(4−3) lines, we have obtained values ranging from 1.4×10^{-2} K km s^{-1} (Model 18) to 1.6 K km s^{-1} (Model 16).

Acknowledgements. E.B. acknowledges financial support from the Leverhulme Trust. We thanks the referee for the useful comments.

References

Bell, T. A., Viti, S., Williams, D. A., Crawford, I. A., & Price, R. J. 2005, MNRAS, 357, 961
Bell, T. A., Viti, S., & Williams, D. A. 2007, MNRAS, 378, 983
Bayet, E., Viti, S., Williams, D. A., Rawlings, J. M. C., & Bell, T. 2009, ApJ, 696, 1466
Conselice, C. J., Gallagher, III, J. S., & Wyse, R. F. G. 2001, AJ, 122, 2281
Crawford, C. S., & Fabian, A. C. 1992, MNRAS, 259, 265
Crawford, C. S., Allen, S. W., Ebeling, H., Edge, A. C., & Fabian, A. C. 1999, MNRAS, 306, 857
de Jong, T., Boland, W., & Dalgarno, A. 1980, A&A, 91, 68
Ferland, G. J., Fabian, A. C., Hatch, N. A., et al. 2008, MNRAS, 386, L72
Ferland, G. J., Fabian, A. C., Hatch, N. A., et al. 2009, MNRAS, 392, 1475
Habing, H. J. 1968, Bull. Astron. Inst. Netherlands, 19, 421
Ho, I.-T., Lim, J., & Dinh-V-Trung 2009, ApJ, 698, 1191
Jaffe, W., Bremer, M. N., & Baker, K. 2005, MNRAS, 360, 748
Johnstone, R. M., Hatch, N. A., Ferland, G. J., et al. 2007, MNRAS, 382, 1246
Lee, H., Herbst, E., Pineau des Forets, G., Roueff, E., & Le Bourlot, J. 1996, A&A, 311, 690
Lepp, S., & Dalgarno, A. 1996, A&A, 306, L21
Lepp, S., & Tiné, S. 1998, The Molecular Astrophysics of Stars and Galaxies, ed. T. W. Hartquist, & D. A. Williams (Oxford: Clarendon Press), 4, 489
Lim, J., Ao, Y., & Dinh-V-Trung 2008, ApJ, 672, 252
McNamara, B. R., O'Connell, R. W., & Sarazin, C. L. 1996, AJ, 112, 91
Pope, E. C. D., Hartquist, T. W., & Pittard, J. M. 2008a, MNRAS, 389, 1259
Pope, E. C. D., Pittard, J. M., Hartquist, T. W., & Falle, S. A. E. G. 2008b, MNRAS, 385, 1779
Rawlings, J. M. C., Hartquist, T. W., Williams, D. A., & Falle, S. A. E. G. 2002, A&A, 391, 681
Röllig, M., Abel, N. P., Bell, T., et al. 2007, A&A, 467, 187
Salomé, P., Combes, F., Edge, A. C., et al. 2006, A&A, 454, 437
Salomé, P., Combes, F., Revaz, Y., et al. 2008a, A&A, 484, 317
Salomé, P., Revaz, Y., Combes, F., et al. 2008b, A&A, 483, 793
Sanders, J. S., & Fabian, A. C. 2007, MNRAS, 381, 1381
Sanders, J. S., Fabian, A. C., Allen, S. W., & Schmidt, R. W. 2004, MNRAS, 349, 952
Schöier, F. L., van der Tak, F. F. S., van Dishoeck, E. F., & Black, J. H. 2005, A&A, 432, 369
van der Tak, F. F. S., Black, J. H., Schöier, F. L., Jansen, D. J., & van Dishoeck, E. F. 2007, A&A, 468, 627

[1] http://www.sron.rug.nl/vdtak/radex/radex.php